Journal of Engineering and Applied Sciences 13 (Special Issue 14): 11006-11023, 2018
ISSN: 1816-949X

Natural Convection Visualization by Heatline for Nanofluids Inside a Square Enclosure Having a Concentric Inner Circular Cylinder at Isoflux Heating Condition on Bottom Wall

Hameed K. Hamzah, Qusay Rasheed Al-Amir, Mohammed Y. Jabbar and Farooq H. Ali
Department of Mechanical Engineering, College of Engineering, University of Babylon, Babylon, Iraq

Abstract: In the current research, natural convection visualization by heatline inside a square enclosure filled with or without nanofluid having concentric inner circular cylinder was numerically investigated under steady and unsteady state conditions. The nanofluid considered was copper nanoparticles dispersed in water. The vertical walls of this enclosure were cooled and the bottom wall was subjected to isoflux heating condition while the upper wall and circular cylinder were insulated. The COMSOL Multiphysics Software 5.2a was utilized to simulate the dimensionless governing equations. These equations were discretized by finite-element techniques. Calculations were achieved for solid volume fractions (0, 0.05, 0.1, 0.15 and 0.2), position of heating element $(0.2L<\zeta<0.5L)$, heating element length ratios ($0.2<\varepsilon<0.8$) and the Rayleigh number ($10^3 \leq Ra \leq 0^6$). Impermanent growth of thermal layer inside the enclosure filled with nanofluid was simulated from initial to steady state. At $\tau = 0.1$, the maximum temperature reached its steady state for higher Rayleigh number (10^5-10^6) while for lower Rayleigh number (10^4), it reached to steady state when time histories increased to about 0.8. Results revealed that changing the position and length of heating element have considerable effects on isotherms, streamlines and heatlines patterns. In addition, the average Nusselt number increases with increasing the nanoparticle volume fractions for any value of Rayleigh number. This research is coincided with other available in the literature.

Key words: Nanofluids, natural convection, unsteady state condition, square enclosure, heatlines, heat flux

INTRODUCTION

The phenomena of steady and unsteady state of convection heat transfer inside closed enclosures are essential in several purposes such as air conditioning of buildings, nuclear reactors, solar energy, electronic equipment's, grain storage and other energy technologies. Additional applications are shown by Choi and Eastman (1995), Xuan and Li (2000) and Xie *et al*. (2002). Most liquids like water and oils have low thermal conductivity which can be enhanced by adding the solid nanoparticles (sized 1-100 nm) to the base fluid. Thus, these fluids are called nanofluids and is investigated widely throughout the recent years Abu-Nada *et al*. (2010), Khodadadi and Hosseinizadeh (2007) and Sivasankaran and Pan (2014). Until now, researches conflict about how the nanoparticle affects the heat transfer, some researchers, for example, Putra *et al*. (2003) described that the nanofluids have heat transfer coefficient less than that for a clear fluid but other researchers, for example, Oztop and Abu-Nada (2008) and Oztop *et al*. (2012, 2015) described that the presence of nanoparticles in the based fluid leads to improve the heat transfer characteristics.

Zhao *et al*. (2007) analyzed the fluid flow and heat transfer characteristics through the streamlines and heatlines across squre enclosures. Nguyen *et al*. (2016) have been spent to examine the unsteady stale effect with different heat source configurations at the bottom. Natural convection in a right-angle triangular cavity heated from bottom wall was studied by Ghasemi and Aminossadati (2010a, b). They used Ethylene Glycol-Cu nanofluid in their investigate. Results indicated that there is an optimum value of solid volume fraction for high values of Rayleigh number. Another study was presented by Aminossadati and Ghasemi (2010a, b), to investigate the periodic natural convection heat transfer within a nanofluids-filled cavity. The oscillating heat flux source was placed on the left wall of cavity whereas the right wall was cold and the other walls were insulated. Their results indicated that the using of Cu nanoparticles improves the thermophysical properties, especially, at lower value of Ra

Corresponding Author: Farooq H. Ali, Department of Mechanical Engineering, College of Engineering, University of Babylon, Babylon, Iraq

number. A numerical study by Jmai *et al.* (2013) was carried out within a square cavity containing various types of nanoparticles. The cavity was partially heated at vertical walls. Results of their study showed that using the volume fraction of nanoparticles caused an increase in heat transfer rate when Ra number increases.

Rahman *et al.* (2016) carried out a computational study of unsteady nutural convection in non-uniformly heated isosceles triangular cavity containing Al_2O_3-water nanofluid. Parameters used in their studied were solid volume fraction, aspect ratio, Rayleigh number and dimensionless time. Results explained that the flow strength becomes constant with dimensionless time at small values of aspect ratio for all studied cases. The strength of the streamlines decreased with increasing of nanoparticles volume fraction. A numerical analysis of free convection inside cavity with inclined heater under unsteady state was conducted by Rahman *et al.* (2014). They indicated that there was linear connection between Nu and Ra. Roslan *et al.* (2014), analysed numerically the free convection inside a square enclosure with differentially heated having a polygon object. The considered parameters in their study were the Rayleigh number ($10^3 \leq Ra \leq 10^6$), polygon type ($3 \leq N \leq \infty$), the polygon size ($0 \leq A \leq \pi/16$), the horizontal location ($0.25 \leq X_0 \leq 0.75$) and the thermal conductivity ratio ($0.1 \leq K_r \leq 10$). The results revealed that the rate of heat transfer increases by increasing polygon size, till it reaches its critical value. Then, the rate of heat transfer decreased beyond the critical value of the polygon size. Heat functions techniques were used by Hussein and Hussain (2016), to depict the natural convection inside wavy cavities. These cavities were filled with Ag-water and Al_2O_3-water nanofluids. Furthermore, the local Nusselt number along the heater increases when the wave amplitudes and solid volume fractions increase. Saeid (2018) investigated the effect of various fin shapes on free convection in a square enclosure. Fin shapes represent by small heating strip located at the bottom wall. He found either the height of the fins or increasing the Grashof number enhancing the heat transfer. Mohebbi *et al.* (2017) used the lattice Boltzmann method in their mathematical modeling and reported the effect of the position of heater on natural convection in a C-shaped enclosure nanofluid-filled. According to the results, the maximum Nu number was attained at lower Ra (10^3) when the heater was placed in the upper horizontal cavity. Furthermore, the heater locations inside the cavity give the best Nu numbers at higher Ra (10^6). Different properties of Al_2O_3-water nanofluid such as variable thermal conductivity, viscosity and the thermal expansion coefficient was used by Ghahremani (2018) to study the transient natural convection inside an enclosure. He concluded that by increasing the solid volume fraction, the flow development time showed different behaviors for various Rayleigh numbers. Enhancing the nanoparticles concentration leads to decrease the flow development time. Ghasemi and Aminossadati (2010a, b) studied free convection cooling of a heater located on the bottom wall of an enclosure. The upper wall and vertical walls of the enclosure were fixed at cold temperature. They showed that the addion of nanoparticles into pure water improved its cooling performance at lower Ra number. Alsabery *et al.* (2017) conducted numerically the transient natural convection within a trapezoidal cavity containing non-Newtonian nanofluid. The cavity subjected to sinusoidal boundary conditions on both sidewalls. The results explained that the rate of heat transfer ries considerably by both higher sidewall inclination angles and the addition of phase deviation.

From open literature, there is no work, until now deals with unsteady natural convection inside the square enclosure containing insulated inner circular cylinder using heatline approach. Also, the current study is made to examine the effects of the solid volume fraction and Rayleigh number as well as effects of position and length ratio of heat element (ε) on the fluid flow and heat transfer within the enclosure under unsteady state conditions.

Problem description: The square enclosure scheme is shown in Fig. 1. Two vertical walls in this enclosure are cooled at fixed temperature and isoflux heating element (q") is placed on the bottom wall while the upper wall and inner circular cylinder are adiabatic boundary. The ratio between cylinder Diameter (D) and enclosure Length (L) equals 0.4 and also the ratio between length of heating element (B) to the length of enclosure is expressed by the index (ε). Furthermore, some assumptions are offered:

- The heating element position is expressed by (ζ) which is measured from the left side of a vertical wall towards the vertical mid-axis of the enclosure
- The Boussines q approximation is invoked in y-direction only
- Nanofluids suggested in the study are incompressible, Laminar flow and Newtonian
- The nanoparticles have a uniform profile and size
- Thermal equilibriums are presented between the water and copper nanoparticles
- Radiation effects are neglected on the both of walls temperature and cylinder

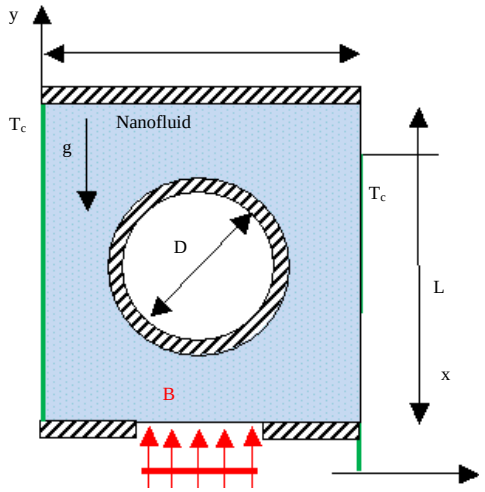

Fig. 1: Square enclosure scheme with boundary conditions

Mathematical modeling

Governing equations: Two-dimensional equations (conservation of mass, momentum and energy) for unsteady natural convection inside the square enclosure are simplified according to above assumptions. The dimensionless forms of these equations can be written as following (Rahman *et al*., 2014, 2016):

$$X=\frac{x}{L};\ Y=\frac{y}{L};\ U=\frac{uH}{\alpha_f};\ v=\frac{vL}{\alpha_f};\ P=\frac{pL^2}{\rho_f\alpha_f{}^2}\theta=\frac{T-T_c}{\Delta T};\ \tau=\frac{t\alpha_f}{L^2};\ \Delta T=\frac{qL}{k_f};\ Ra=\frac{g\,\beta_f(\nabla T)L^2}{\alpha_f\nu_f};\ Pr=\frac{\nu_f}{\alpha_f}$$

$$\frac{\partial U}{\partial X}+\frac{\partial V}{\partial Y}=0 \tag{1}$$

$$\frac{\partial U}{\partial \tau}+U\frac{\partial U}{\partial X}+V\frac{\partial U}{\partial Y}=-\frac{\partial P}{\partial X}+\frac{\mu_{nf}}{\rho_{nf}\alpha_f}\left(\frac{\partial^2 U}{\partial X^2}+\frac{\partial^2 U}{\partial Y^2}\right) \tag{2}$$

$$\frac{\partial V}{\partial \tau}+U\frac{\partial V}{\partial X}+V\frac{\partial V}{\partial Y}=-\frac{\partial P}{\partial Y}+\frac{\mu_{nf}}{\rho_{nf}\alpha_f}\left(\frac{\partial^2 V}{\partial X^2}+\frac{\partial^2 V}{\partial Y^2}\right)+\frac{(\rho\beta)_{nf}}{\rho_{nf}\beta_f}Ra\,Pr \tag{3}$$

$$\frac{\partial \theta}{\partial \tau}+U\frac{\partial \theta}{\partial X}+V\frac{\partial \theta}{\partial Y}=-\frac{\alpha_{nf}}{\alpha_f}\left(\frac{\partial^2 \theta}{\partial X^2}+\frac{\partial^2 \theta}{\partial Y^2}\right) \tag{4}$$

where, α_{nf}, ρ_{nf} and μ_{nf} are thermal diffusivity, the effective density and the effective dynamic viscosity (Brinkman, 1952) of the nanofluid, respectively which are given by:

Table 1: Thermo-physical properties of pure water and copper nanoparticles

Properties	k (W/m.k)	ρ (kg/m^3)	β (1/k)	C_p (J/kg k)	μ (kg/msec)
Copper (Cu)	401	8933	1.67×10^{-5}	385	-
Pure water	0.613	997.1	21×10^{-5}	4179	0.000372

$$\alpha_{nf}=\frac{k_{nf}}{(\rho C_p)_{nf}} \tag{5}$$

$$\rho_{nf}=(1-\varphi)\rho_f+\varphi\rho_p \tag{6}$$

$$\mu_{nf}=\frac{\mu_f}{(1-\varphi)^2}.5 \tag{7}$$

where, also, k_{nf} and φ are the effective thermal conductivity and solid volume fraction of nanofluid, respectively. For spherical nanoparticles, the k_{nf} is defined by Maxwell (1904):

$$k_{nf}=k_f\left(\frac{(k_p+2k_f)-2\varphi(k_f-k_p)}{(k_p+2k_f)+\varphi(k_f-k_p)}\right) \tag{8}$$

Furthermore, the thermal expansion coefficient $(\beta)_{nf}$ and heat Capacitance $(C_p)_{nf}$ of the nanofluid are given by:

$$(\rho\beta)_{nf}=(1-\varphi)(\rho\beta)_f+\varphi(\rho\beta)_p \tag{9}$$

$$(\rho C_p)_{nf}=(1-\varphi)(\rho C_p)_f+\varphi(\rho C_p)_p \tag{10}$$

The values of thermo-physical properties of the pure water and the Copper nanoparticles are reported by Mahmoodi and Sebdani (2012) which are given in Table 1 The local Nusselt number on the heating element is known as following:

$$Nu_s=\frac{hL}{k_f} \tag{11}$$

where, h is the heat transfer coefficient which is given as:

$$h=\frac{q''}{T_s-T_c} \tag{12}$$

Using dimensionless parameters, the local Nusselt number becomes:

$$Nu_s=\frac{1}{\theta|_{\text{wall of heating element}}} \tag{13}$$

By integration of local Nusselt number (Nu_s) along the heating element, the average Nusselt number $(\overline{Nu_s})$ is calculated as:

$$\left(\overline{Nu_s}\right) = \frac{1}{B}\int_N^M Nu_s(X)dX \quad (14)$$

Stream and heat functions: The fluid flow is exhibitted using the stream function (ψ) getted from components of velocity (U and V). For two-dimensional flow, relations between stream function, ψ (Basak *et al*., 2010a, b) and components of velocity are as following:

$$U = \frac{\partial \psi}{\partial Y}, \quad V = -\frac{\partial \psi}{\partial X} \quad (15)$$

$$\frac{\partial^2 \psi}{\partial X^2} + \frac{\partial^2 \psi}{\partial Y^2} = \frac{\partial U}{\partial Y} - \frac{\partial V}{\partial X} \quad (16)$$

On all walls, the no-slip boundary condition is applied ($\psi = 0$) at the nodes for the boundaries. On the other hand, the dimensionless heat function (Π) is used to visualize heat flow in the enclosure which is obtained from convective heat fluxes ($U\theta$, $V\theta$) and conductive (diffusive) heat fluxes ($-\partial\theta/\partial X$-$\partial\theta/\partial Y$) as following:

$$\frac{\partial \Pi}{\partial Y} = U\theta - \frac{\alpha_{nf}}{\alpha_f}\frac{\partial \theta}{\partial X}, \quad -\frac{\partial \Pi}{\partial X} = V\theta - \frac{\alpha_{nf}}{\alpha_f}\frac{\partial \theta}{\partial Y} \quad (17)$$

This function satisfies the steady state energy Eq. 18 (Basak *et al*., 2010a, b) as following:

$$\frac{\partial^2 \Pi}{\partial X^2} + \frac{\partial^2 \Pi}{\partial Y^2} = \frac{\partial}{\partial Y}(U\theta) - \frac{\partial}{\partial X}(V\theta) \quad (18)$$

The heat function boundary conditions are derived from Eq. 17:

Initial and boundary conditions: These conditions can be also modified in dimensionless parameters as follows:

Initial conditions ($\tau = 0$): $\theta = 0$; $U = 0$; $V = 0$. In the present study, the governing equations (1, 2, 3, 4, 16 and 18) with boundary conditions are arranged as following:

Boundary conditions ($\tau > 0$): For left vertical wall ($X = 0$ and $0 \le Y \le 1$) for right vertical wall ($X = 1$ and $0 \le Y \le 1$) the velocity components, dimensionless temperature, stream and heat functions after substituted become:

$$U = 0;\ V = 0;\ \theta = 0,\ \psi = 0,\ n.\nabla\Pi = 0$$

For bottom wall three regiions can be recognized: the first region ($Y = 0$ and $0 \le X \le M$):

$$U = 0;\ V = 0;\ \frac{\partial \theta}{\partial Y} = 0,\ \psi = 0,\ \Pi = 0$$

The second region ($Y = 0$ and $N \le X \le 1$):

$$U = 0;\ V = 0;\ \frac{\partial \theta}{\partial Y} = 0,\ \psi = 0,\ n.\nabla\Pi = 0$$

The third region ($Y = 0$ and $M \le X \le 1$):

$$U = 0;\ V = 0;\ \frac{\partial \theta}{\partial Y} = -\frac{K_f}{K_{nf}},\ \psi = 0,\ -\frac{\partial \Pi}{\partial X} = \frac{k_f}{k_{nf}}\frac{\alpha_{nf}}{\alpha_f}$$

where, $M = 0.5(1-\varepsilon)$ and $N = 0.5(1+\varepsilon)$. For upper wall ($Y = 1$ and $0 \le X \le 1$):

$$U = 0;\ V = 0;\ \frac{\partial \theta}{\partial Y} = 0,\ \psi = 0,\ n = \int_0^1 \frac{\alpha_{nf}}{\alpha_f}\frac{\partial \theta}{\partial Y}dX$$

For inner cylinder surface:

$$\frac{\partial \theta}{\partial R} = 0,\ \Pi = 0 \text{ and } \psi = 0 \text{ if } \zeta = 0.5L \text{ and}$$
$$\Psi = \Psi_s = \text{constant}, \text{ if } \zeta \neq 0.5L$$

The value of Ψ_s is obtained as follows (Yoo, 1998; Costa and Raimundo, 2010), that is:

$$\psi_s = \left[\int_0^{y_s,\min}(\partial\Psi/\partial y)\right]_{x=0} \quad (19)$$

MATERIALS AND METHODS

Computational methodology: Equation 1, 2, 3, 4, 16 and 18 with initial and boundary conditions are solved computationally by the COMSOL multi-physics software. This software is used finite-element method to discretize these equations. To assure stability, the method so-called Galerkin least-square are utilized. The damped Newton method and a parallel direct solver are implemented to solve the discretized equations.

As shown in Fig. 2, square enclosure was meshed with triangle element. Numerous grid tests were implemented to find the appropriate number of elements for convergence. The convergence criterion used in this study equals 1×10^{-6}. As shown in Table 2, the COMSOL default settings were used to determine mesh sizes. Here, a finer mesh size is selected in the whole calculations which consider on the accuracy and CPU time.

Validation with other works: The beforehand published work on conjugate conduction and natural convection in

a square cavity filled with Cu-water nanofluid ($\varphi = 0.1$) was used to validate the present research. In Fig. 3, the present results are compared against results of

Table 2: Grid sensitivity check for the case $Ra = 10^5$, $\zeta = 0.5L$ and $\varepsilon = 0.4$

Mesh size	Mesh elements	Boundary elements	$\overline{Nu}$	CPU time (sec)
Coarser	653	81	5.5971	5
Coarse	1066	120	5.5732	7
Normal	1609	153	5.5516	6
Fine	2469	193	5.5404	7
Finer	7634	404	5.5242	14
Extra fine	21424	788	5.5201	32
Extremely fine	26934	788	5.5200	32

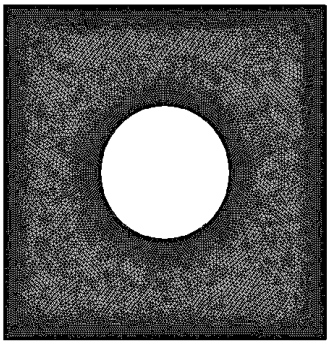

Fig. 2: Mesh distribution of the model

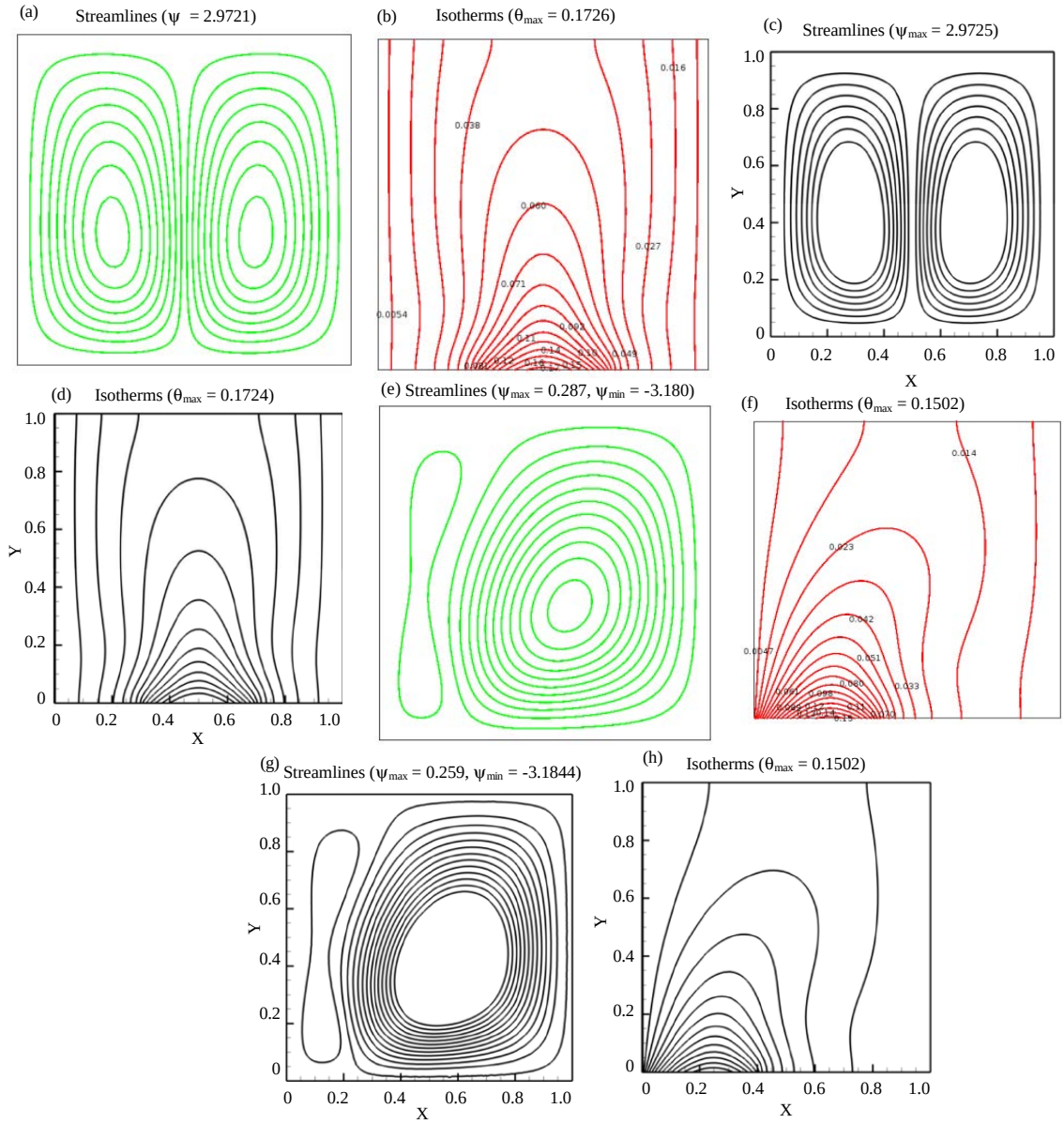

Fig. 3a-h): Comparison isotherms and streamlines both of the present study and Nguyen *et al.* (2016) for cavity at heating element positions ($\zeta = 0.5L$ and $\zeta = 0.2L$); $Ra = 10^5$, $\zeta = 0.5L$, $\varepsilon = 0.4$ $Ra = 10^5$ $\zeta = 0.2L$, $\varepsilon = 0.4$

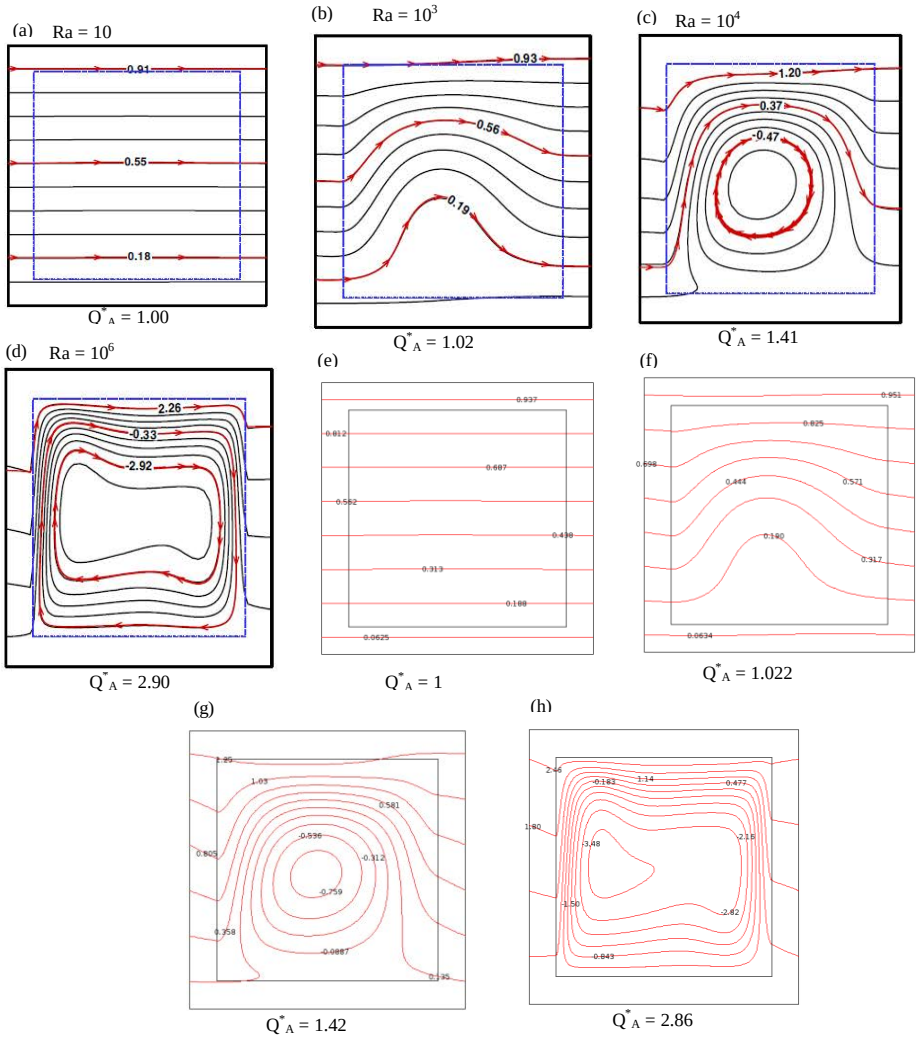

Fig. 4a-h): Comparison of results of heatlines for $\theta = 37$ and $K_r = 1$ in enclosure at different values of Ra (10-10^6) with the corresponding results of Zhao *et al.* (2007) (Present study)

Nguyen *et al.* (2016) for streamlines and isotherms patterns, respectively. Another comparison with results of Zhao *et al.* (2007) is illustrated in Fig. 4 for heatlines contours in a square enclosure at $\theta = 37$ and $K_r = 1.0$ at Rayleigh numbers ranging from 10-10^6. The comparisons make good confidence with present computation.

RESULTS AND DISCUSSION

The effects of position (ζ) and the length ratio of heating element (ε) as well as Rayleigh numbers on the unsteady natural convection within the considered enclosure with nanofluid-filled ($\varphi = 0.1$) or without nanofluid ($\varphi = 0$) are discussed in this investigation. Several values of physical and geometrical parameters used in the study are Rayleigh numbers ($10^3 \leq Ra \leq 10^6$), solid volume fractions of nanoparticles ($0 \leq \varphi \leq 0.2$), heat source positions ($0.2L < \varepsilon < 0.5L$) and the length ratios of heating element ($0.2 < \varepsilon < 0.8$).

Streamlines and isotherms patterns: Figure 5 points out impermanent growth of thermal layer of fluid with dimensionless time (τ) for square enclosure filled with Cu-water nanofluid under constant conditions: $Ra = 10^5$, $\varepsilon = 0.5$ L, , $\varepsilon = 0.4$ and $\varphi = 0.1$. For $\tau = 0.01$, thermal layers of fluid neighboring heating element are heated and formed. These layers move perpendicularly towards the adiabatic circular cylinder in the middle of the enclosure and it spread towards the circumference of cylinder across the two sides of the enclosure ($\tau = 0.11$). These hot layers also continue to rise upward where thermal gradient becomes stronger in the upper part of the adiabatic

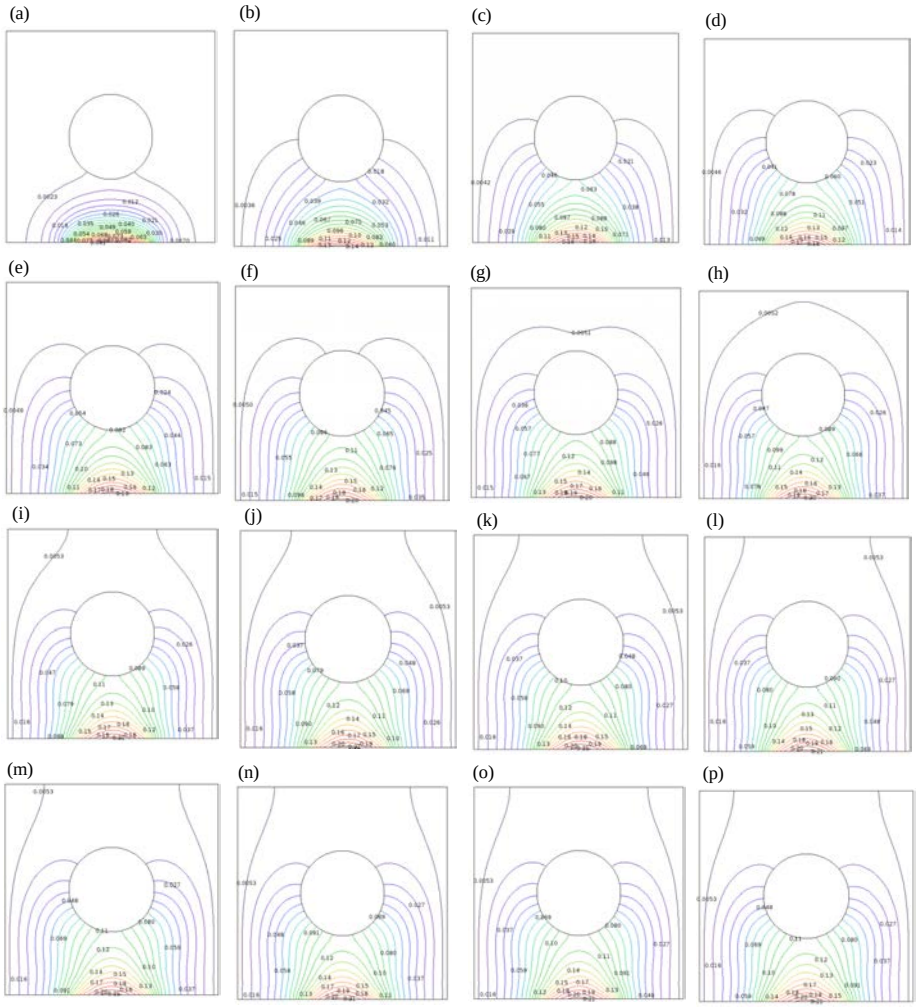

Fig. 5: Isotherms contours of thermal layer with dimensional time t for Ra = 10^5, $\varepsilon = 0.4$, $\zeta = 0.5L$ and $\varphi = 0.1$: a) $\tau = 0.01$; b) $\tau = 0.03$; c) $\tau = 0.05$; d) $\tau = 0.07$; e) $\tau = 0.09$; f) $\tau = 0.11$; g) $\tau = 0.13$; h) $\tau = 0.15$; i) $\tau = 017$; j) $\tau = 019$; k) $\tau = 21$; l) $\tau = 0.23$; m) $\tau = 0.25$; n) $\tau = 0.27$; o) $\tau = 0.29$ and p) $\tau = 1$

circular cylinder as well as its gradient rises more with dimensional time ($\tau = 0.15$). After that it speedily reaches the adiabatic upper wall with dimensional time ($\tau = 0.17$). Then remain in touch with the adiabatic wall and the hot layers travel and spread towards the top wall and distinction in patterns of isotherms are stayed awaiting the steady state is occurred at $\tau = 0.19$.

Figure 6 illustrates the effect of heating element positions ($0.2L<\varepsilon<0.5L$) on the patterns of isotherms and streamlines for enclosure filled with water alone and with water-Cu nanofluid. Patterns of streamlines obviously reveal two irregular rotating cells with uneven strengths dominating the flow field, one of them around the circular cylinder and the other is small in size at corner of enclosure. This happens when the isoflux heating element is placed at distance $\varepsilon = 0.2L$ from the left side wall. Also, the maximum stream function increases for water-Cu nanofluid than that for pure water ($\psi_{max} = 0.281497$ for $\varphi = 0$ and $\psi_{max} = 0.302653$ for $\varphi = 0.1$). As ζ increases 0.3L from to 0.4L, streamlines patterns are the same as those for $\zeta = 0.2L$ but the strength of the circulation cells inside the enclosure increases at both pure water and nanofluid ($\psi_{max} = 0.42777$ to $\psi_{max} = 0.61107$ for $\varphi = 0$, $\psi_{max} = 0.43822$ to $\psi_{max} = 0.59582$ for $\varphi = 0.1$). From final results, the ψ_{max} increases for pure water than that for nanofluid. Further increases of position ($\zeta = 0.5L$) the heating element move from the left wall towards the mid-section of the lower wall, two rotating cells with equal intensity are eventually formed near sides of the adiabatic cylinder inside the enclosure. The stronger in strength of the rotating cells is observed because increase's buoyancy force inside the enclosure. it is still the ψ_{max} increases for pure water than that for nanofluid ($\psi_{max} = 1.8369$ for $\varphi = 0$, $\psi_{max} = 1.2093$ for $\varphi = 0.1$).

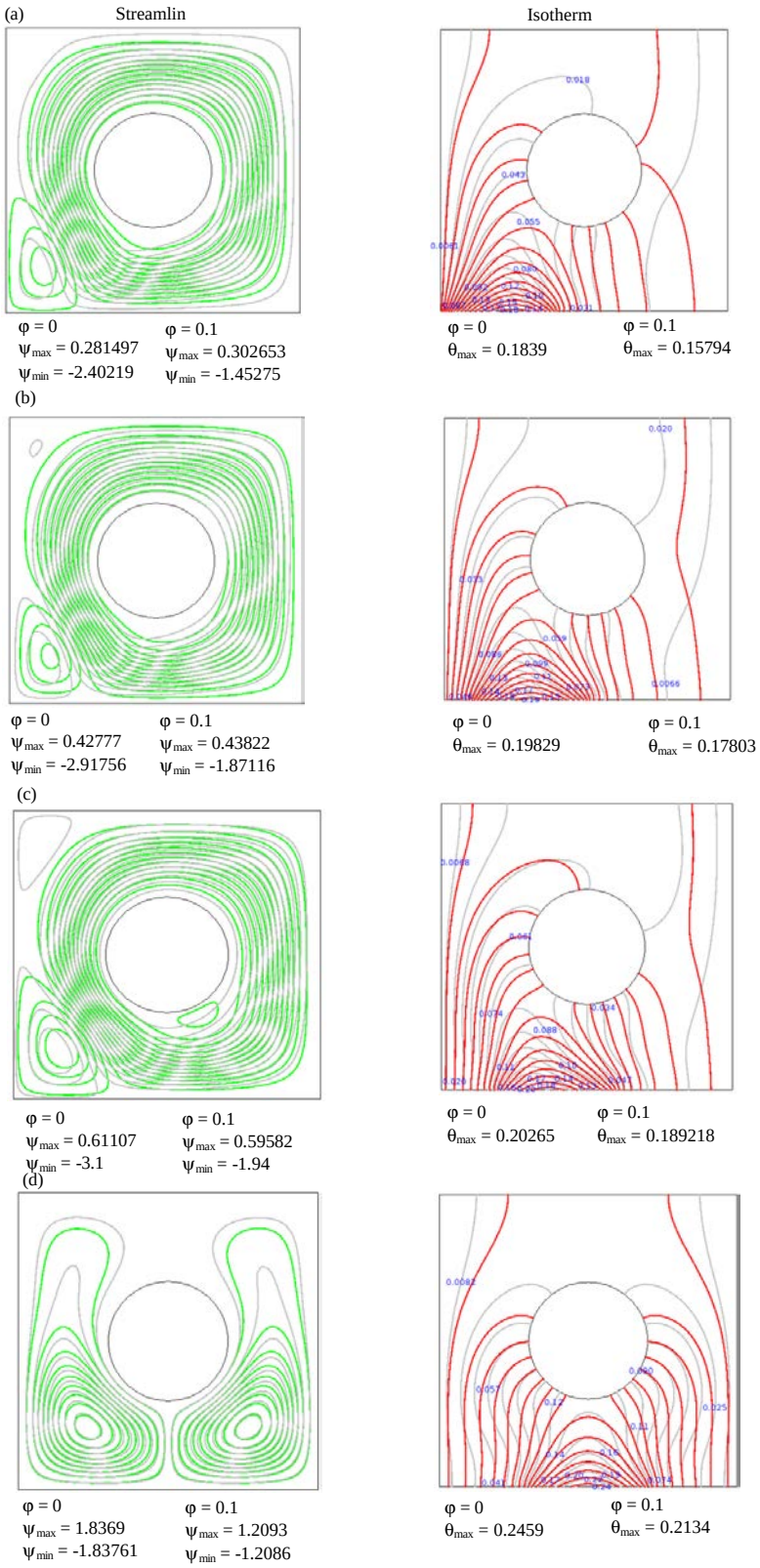

Fig. 6: Streamlines and isotherms patterns for the enclosure filled with water (light line) and water-Cu nanofluid (dark line) at different heating element positions (Ra = 10^5 and ε = 0.4L): a) ζ = 0.2L; b) ζ = 0.3L; c) ζ = 0.4L and d) ζ = 0.5L (Position)

Similar streamlines patterns are observed in isotherms patterns as the heating element is moved. The isotherms patterns are similar in shape when the positions of heating element increase from to However, the maximum temperature increases in both pure water and nanofluid (θ_{max} = 0.1839-0.20265 for φ = 0, θ_{max} = 0.15794-0.189218 for φ = 0.1). This leads to decrease in rate of heat transfer at the surface of heating element. Further increases in the heating element position from to the θ_{max} increases and becomes highest for both of pure water and nanofluid (θ_{max} =0.2459 for φ = 0, θ_{max} = 0.2134 for φ = 0.1). Consequently, the heating element closest to the left cold wall, the heat transfer rate becomes the great. The circular cylinder at the center causes increase in temperature distribution in enclosure.

Figure 7 points out patterns of streamlines and isotherms in the enclosure for both water (φ = 0) and water-Cu nanofluid (φ = 0.1) at Ra = 10^5, and different ratios of heating element length (ε) namely 0.2, 0.4, 0.6 and 0.8, respectively. When ε = 0.2, two circulating cells of the same sizes are observed in the flow field. It also observed that the maximum stream function increases more for water than that for nanofluid (ψ_{max} = 1.09991 for φ = 0, ψ_{max} = 0.642446 for φ = 0.1). Streamline patterns are similar in shape at other ratios of heating element but the intensity of circulation cells gradually increase as the ratios of heating element length increase from 0.4-0.8, respectively (ψ_{max} = 1.8369 to ψ_{max} = 2.63326 for pure water, ψ_{max} = 1.2093 to ψ_{max} = 1.84921 for nanofluid). The results of isotherms patterns show that the maximum temperature increases from θ_{max} = 0.1781 to θ_{max} = 0.313018 for pure water (φ = 0) and from θ_{max} = 0.143 to θ_{max} = 0.28384 for nanofluid (φ = 0.1) as the ratios (ε) increase from 0.2-0.8, respectively.

Figure 8 illustrates the streamlines and isotherms patterns for pure water (φ = 0) and water-Cu nanofluid (φ = 0.1) at ε = 0.4 and ζ = for different Rayleigh numbers (10^3, 10^4, 10^5 and 10^6). The strength of the flow field reduces when the nanoparticles added to a pure water (φ) for all values of Ra. At low Rayleigh numbers

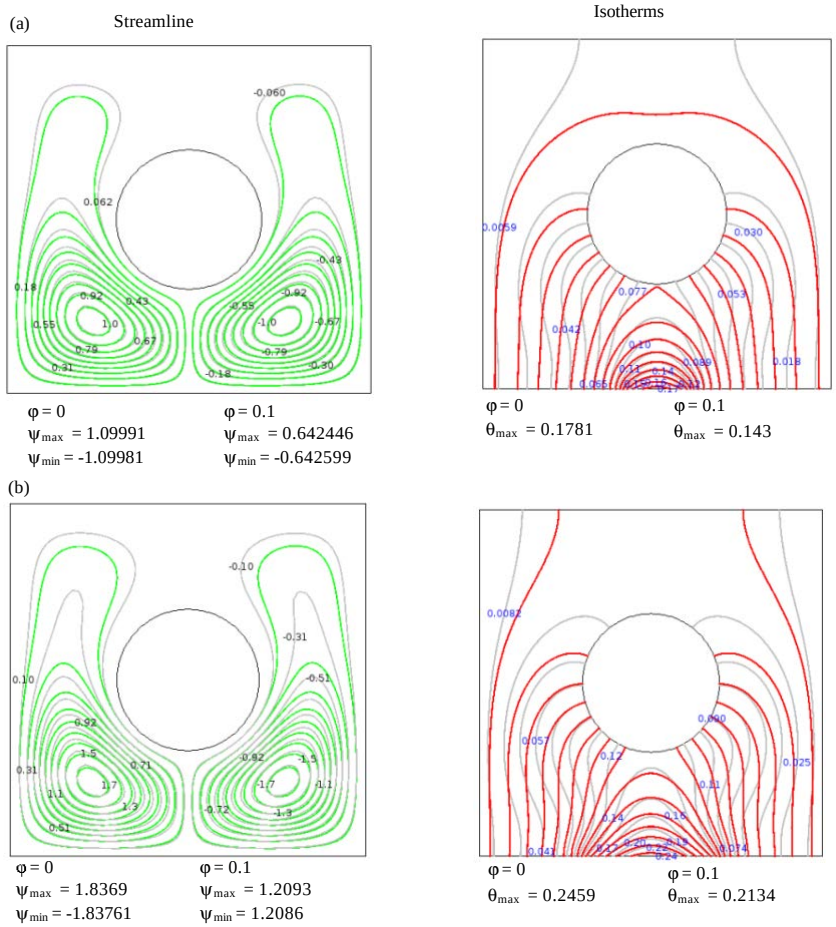

Fig. 7: Continue

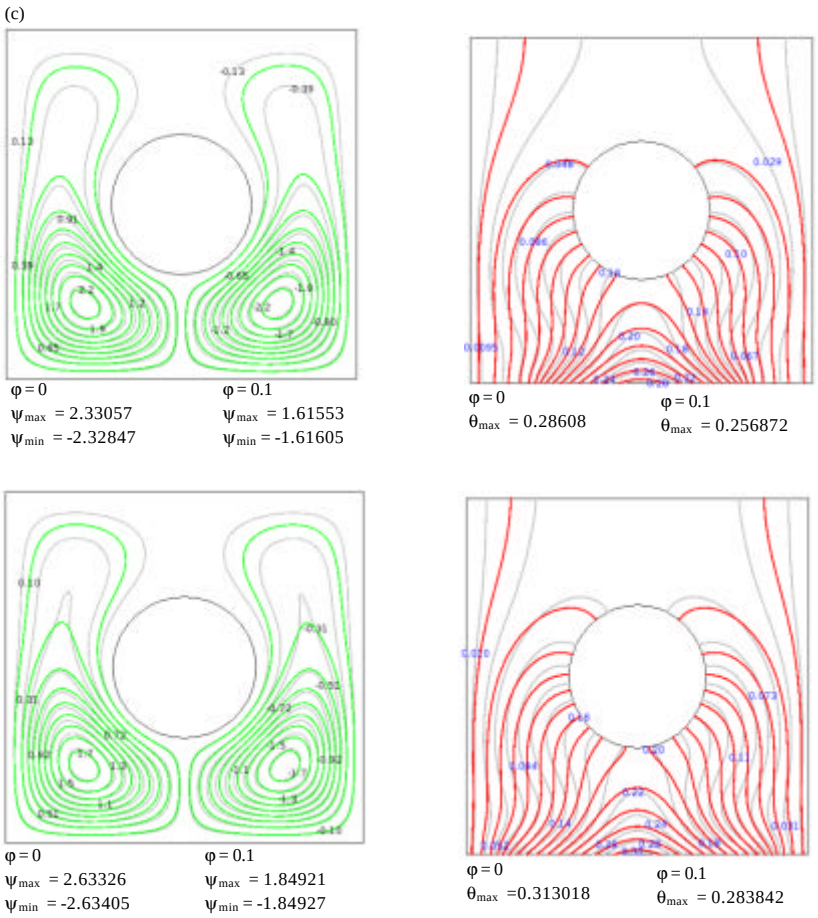

Fig. 7: Streamlines and isotherms patterns for the enclosure filled with water, φ = 0 (light line) and with nanofluid, φ = 0.1 (dark line) at different heating element lengths (Ra = 10^5 and ζ = 0.5L): a) ε = 0.2; b) ε = 0.4; c) ε = 0.6 and d) ε = 0.8

(Ra = 10^3), the fluid motion is weak inside the enclosure due to its lower effect of the buoyancy force. The streamlines patterns in this case observe two rotating eddies. These cells have lower values of maximum stream function (ψ_{max} = 0.020079 for φ = 0 and ψ_{max} = 0.0122 for φ = 0.1). Hence, heat transfer by conduction is dominated in the flow field when Rayleigh number increases to 10^4, the buoyancy effect is still weak. Therefore, the streamlines patterns are almost symmetric as compared to prior Ra for both of pure water and nanofluid despite some differences in magnitudes of maximum stream function between two Ra numbers (ψ_{max} = 0.2089 for φ = 0 and ψ_{max} = 0.114298 for φ = 0.1). The effect of buoyancy force becomes larger when Ra increases to 10^5. The natural convection becomes more considerable. With the further increase in Ra (Ra = 10^6), the flow strengthens and the maximum stream function values increase more (ψ_{max} = 6.2613 for φ = 0 and ψ_{max} = 5.57835 for φ = 0.1). Isotherms patterns show that the addition of nanoparticles reduces the maximum dimensionless temperature as the Ra increases from 10^3 to 10^6 (θ_{max} = 0.295087-0.133673 for φ = 0, θ_{max} = 0.221495- 0.127561 for φ = 0.1). This reduction in maximum dimensionless temperature improves cooling performance inside the enclosure.

Heatlines patterns: The heatlines patterns represent the path of heat flow within the enclosure which are dissimilar in behaviors from isotherms contour because it comes from intensify thermal mixing. In Fig. 9-12, heat flows emanate from the hot bottom region (heating element) to the cold regions (such as vertical walls) within the enclosure where it stops there. Figure 9 indicates effect of Rayleigh number on the heatlines contours for the case when the enclosure contains pure water (φ = 0). This effect is insignificant at low Rayleigh number (10^3-10^4) where the heat transfer by conduction predominates due to minimal flow activities than the convection and consquently the maximum and minimum values of

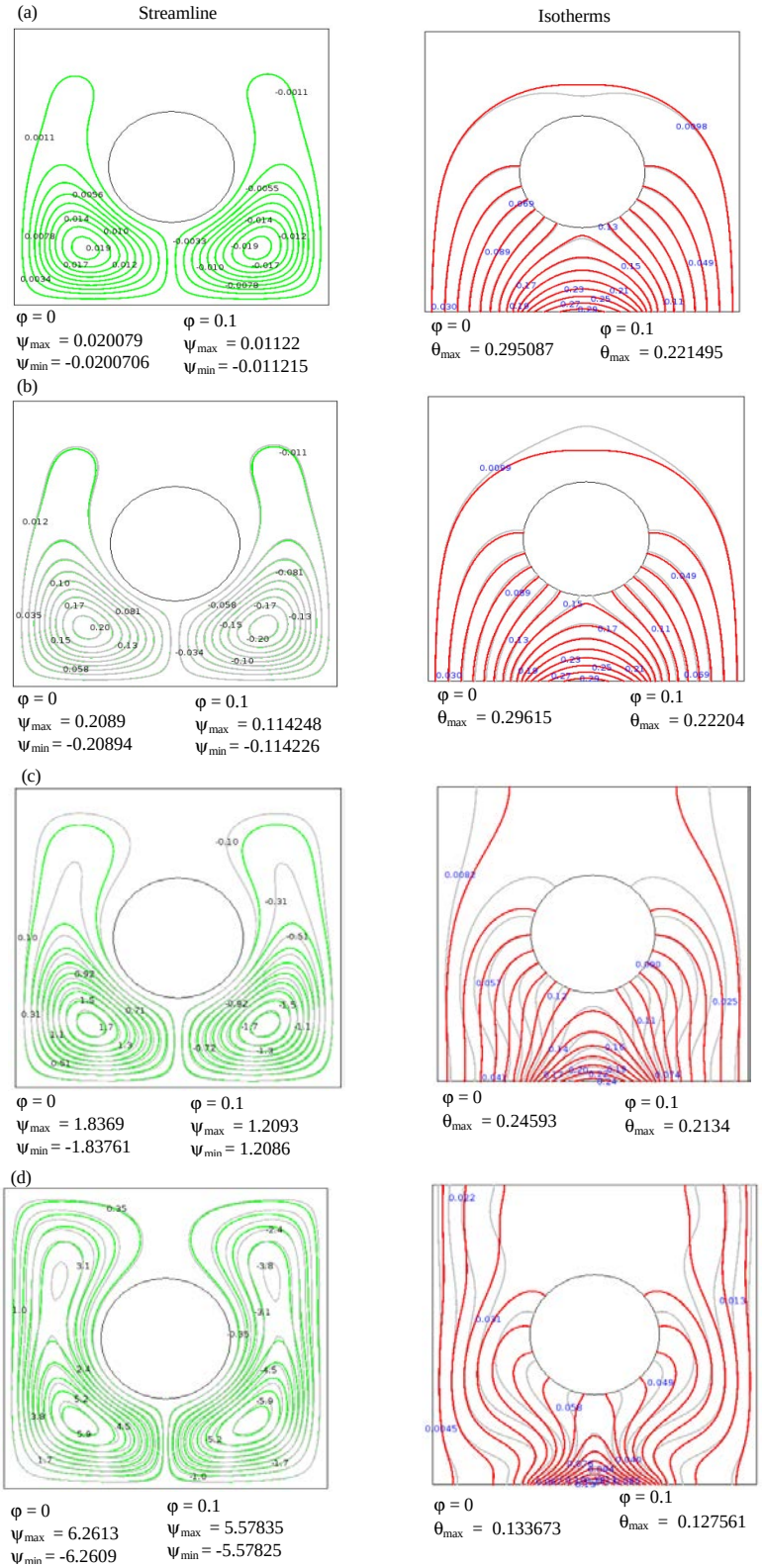

Fig. 8: Streamlines and isotherms patterns for the enclosure filled with water, φ = 0 (light line) and with nanofluid, φ = 0.1 (dark line) at different Rayleigh numbers (ε =0.4 and ζ = 0.5L): a) Ra = 10^3; b) Ra = 10^4; c) Ra = 10^5 and d) Ra = 10^6

dimensionless heat function remain constant (Π_{max} = 0.2 and Π_{min} = - 0.2). When Ra increases from 10^5-10^6, effect of Ra becomes considerable because the natural convection increases with the Ra number inside the enclosure which may result in significant increase in value of maximum heat function (Π_{max} = 0.2595) as shown in final case of Fig. 9. The heatline contours of nanofluid (φ = 0.1) at ε = 0.4 and $\zeta = 0.5L$ for different Rayleigh numbers are showed in Fig. 10. The heat flow from heating element inside the enclosure for natural convection is affected by increasing the Rayleigh number from 10^3-10^5 as shown in Fig. 10. For high Ra number, like Ra = 10^6, heatlines are defaced at left bottom region of the enclosure because of forming a secondary flow near the bottom region from cylinder

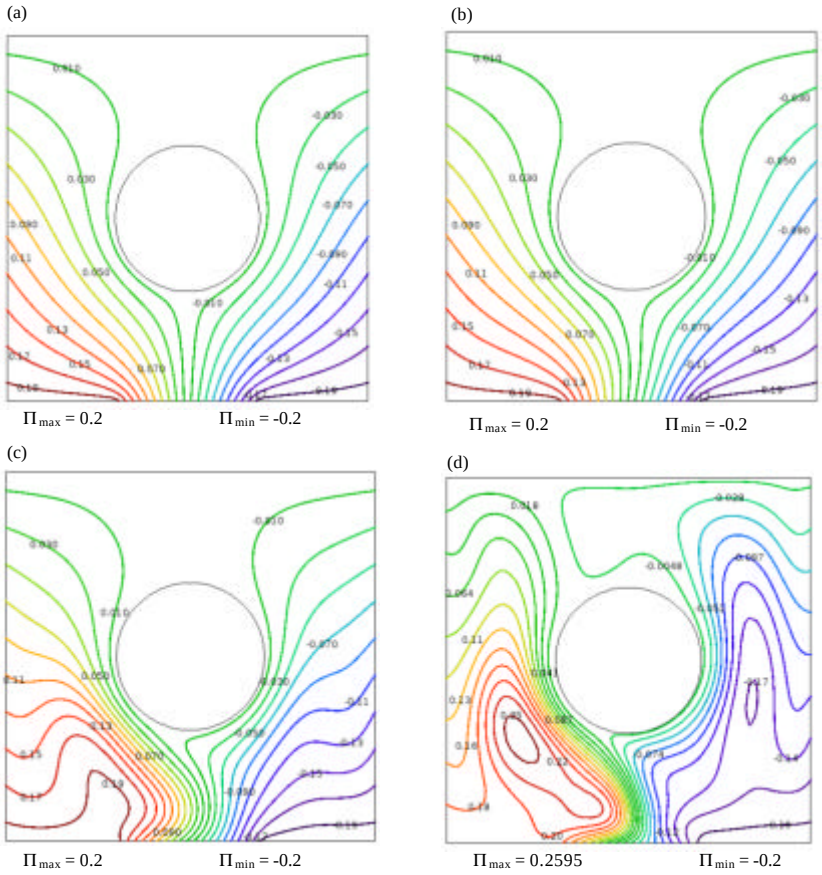

Fig. 9: Heatlines patterns of pure water (φ = 0) at different Rayleigh numbers (ε = 0.4 and · = 0.5L): a) Ra = 10^3; b) Ra = 10^4; c) Ra = 10^5 and d) Ra = 10^6

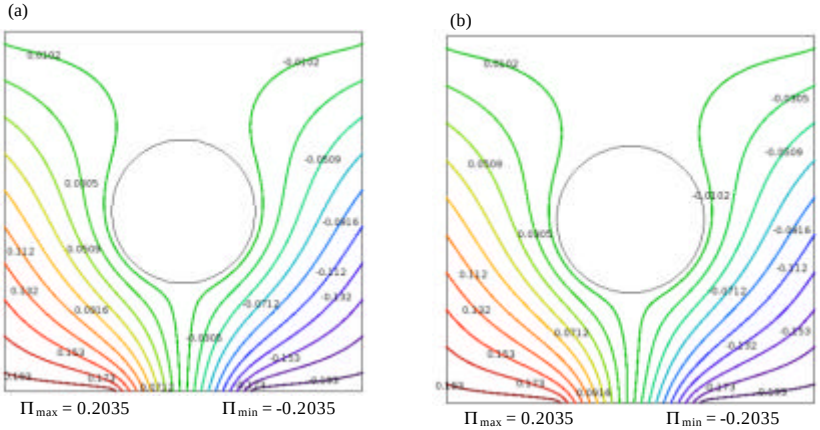

Fig. 10: Continue

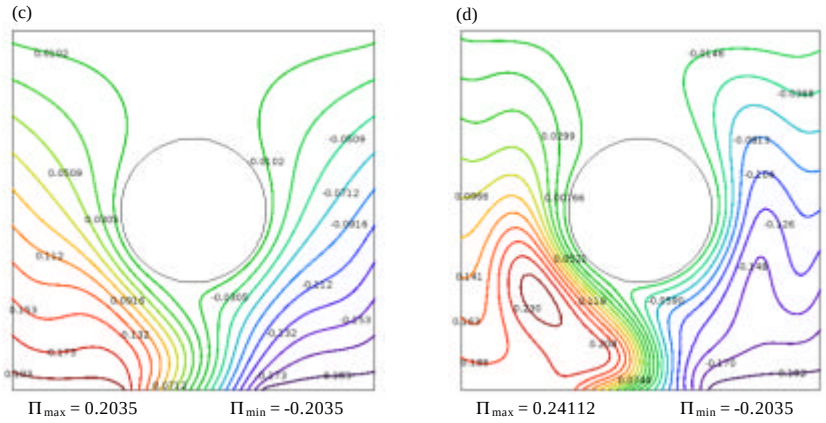

Fig. 10: Heatlines patterns of nanofluid (φ = 0.1) at different Rayleigh numbers (ε =0.4 and · = 0.5L)

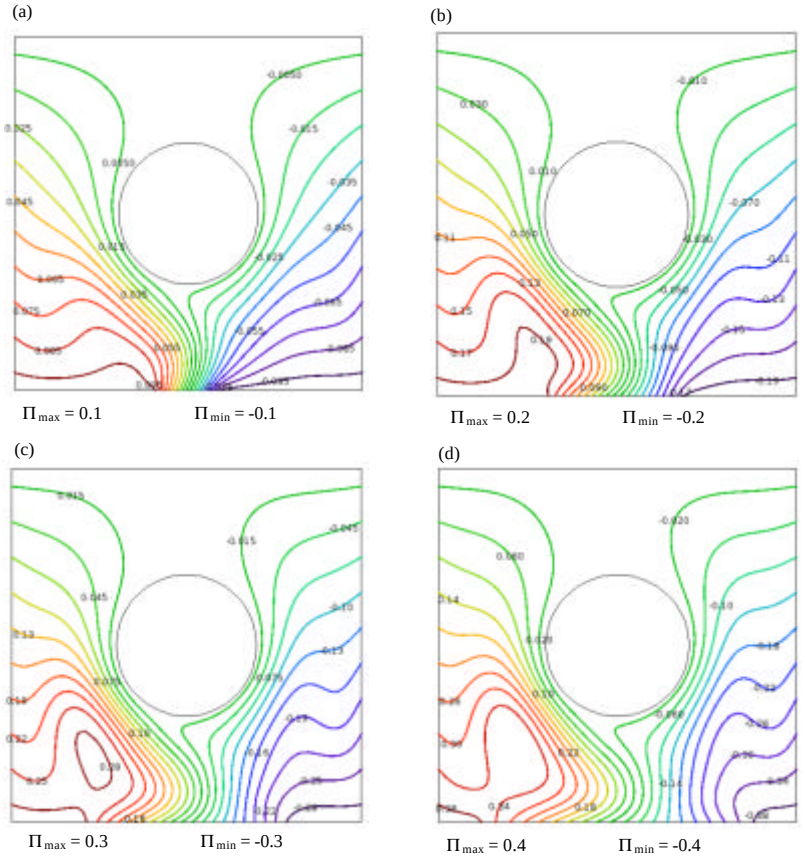

Fig. 11: Heatlines patterns of pure water at different ratios of ε (Ra = 10^5 and ζ = 0.5L): a) ε = 0.2; b) ε = 0.4; c) ε = 0.6 and d) ε = 0.8

surface. Heatline contours of water (φ = 0) and nanofluid (φ = 0.1) are illustrated in Fig. 11 and 12, respectively, for different ratios of heating element length (ε = 0.2, 0.4, 0.6 and 0.8) at Ra = 10^5 and ζ= 0.5L, respectively. It is observed that the shapes of heatline stay unchanged with raitio of ε = 0.2 for both pure water and nanofluid. When the raitio of ε increases from 0.2-0.4, the heatlines start to slope upward at the half bottom of the enclosure more for pure water than that for nanofluid. Another increase of the ratio (ε) from 0.4-0.6, a vortex heating cell is found in the left bottom side of enclosure filled with pure water. On the nanofluid side, the heatlines slope more upward at the

same region with increasing in their intensity. When the heat source length increases so that the ratio (ε) becomes 0.8, heatline contours of pure water and nanofluid relatively have almost same shape. In general, when raitios of heating element length increase from 0.2-0.8, The strength of the heat flow represented by maximum heat function increases for two cases (Π_{max} = 0.1-0.4 for pure water and Π_{max} = 0.10178-0.40711 for nanofluid). Figure 13 and 14 show heatline contours of pure water (φ = 0) and nanofluid (φ = 0.1), respectively for different positions of

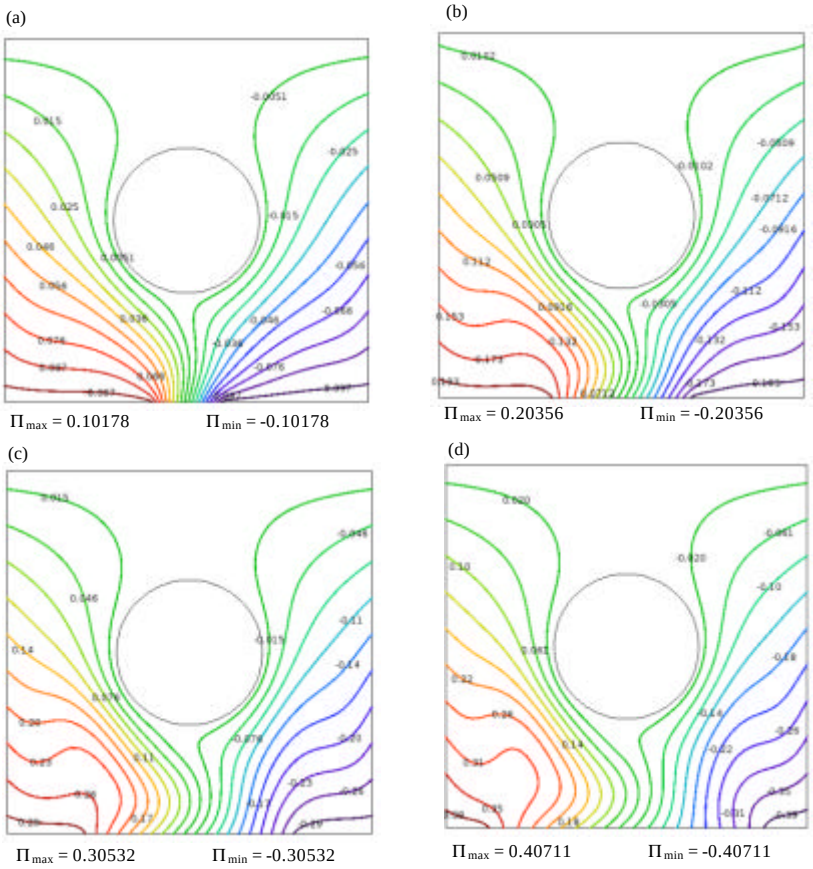

Fig. 12: Heatlines patterns of nanofluid (φ = 0.1) at different different ratios of ε (Ra = 10^6 and ζ = 0.5L): a) ε = 0.2; b) ε = 0.4; c) ε = 0.6 and d) ε = 0.8

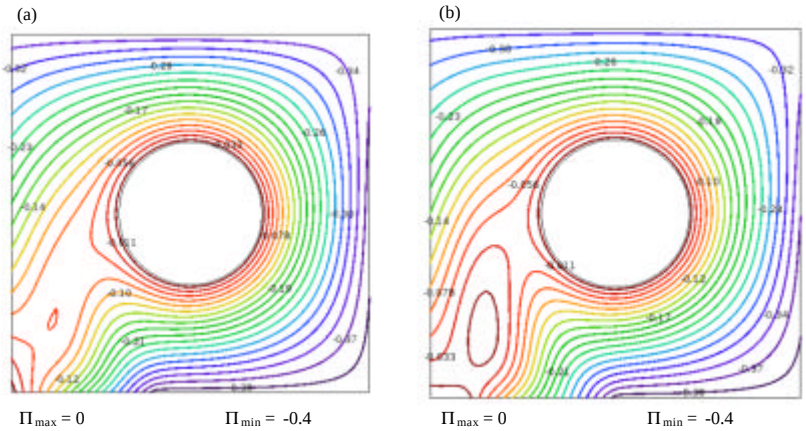

Fig. 13: Continue

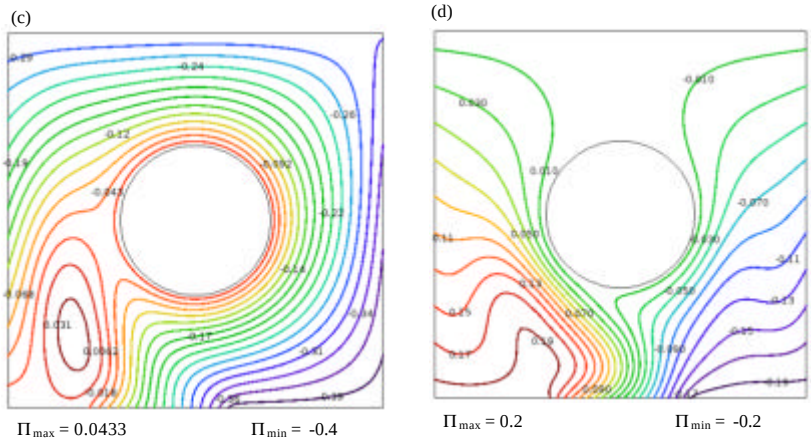

Fig. 13: Heatlines patterns of pure water at different ratios of · (Ra = 10^5 and ε = 0.4): a) · = 0.02L; b) · = 0.3L; c) ζ = 0.4L and d) ζ = 0.5L

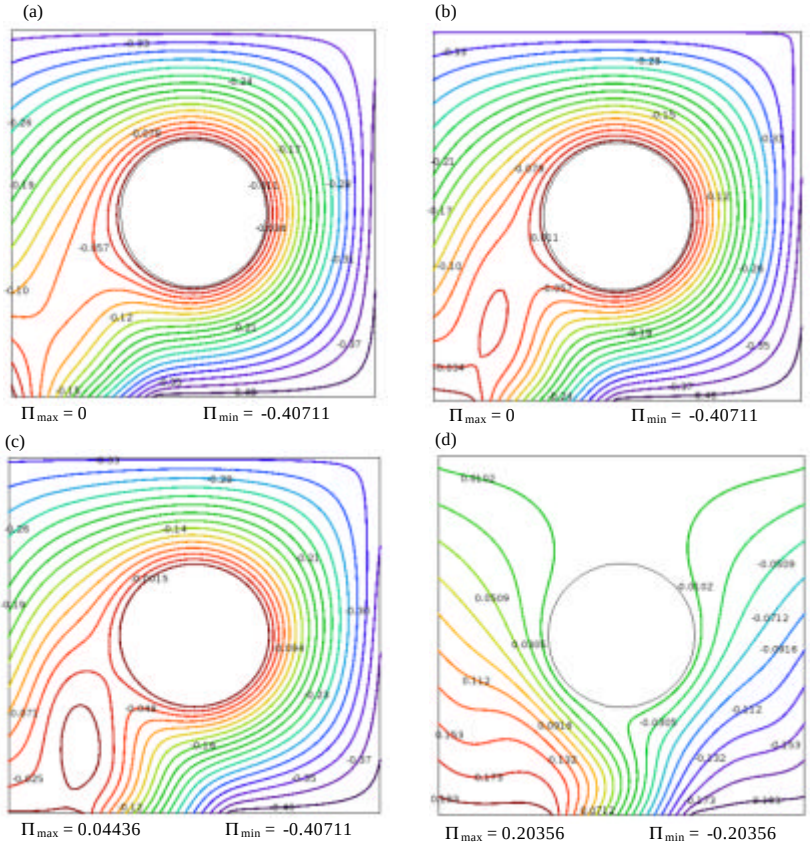

Fig. 14: Heatlines patterns of nanofluid at different ratios of ζ (Ra = 10^5 and ε = 0.4): a) ζ = 0.02L; b) ζ = 0.3L; c) ζ = 0.4L and d) ζ = 0.5L

heating element (ε = 0.2, 0.3, 0.4 and 0.5L) at Ra = 10^5 and θ = 0.4. Similar patterns are observed in heatlines when the heating element position changes from the left vertical wall at position $\zeta = 0.2L$ to position $\zeta = 0.4L$ for both of φ = 0 and φ = 0.1. the direction of heatlines moves around the cylinder towards the cold left sidewall from the hot region. When the position of heating element changes from position $\zeta = 0.4L$ to the center of the mid-section at position $\zeta = 0.5L$ the heat function increases from (Π_{max} = 0.0433) to (Π_{max} = 0.2) for pure water and they increase

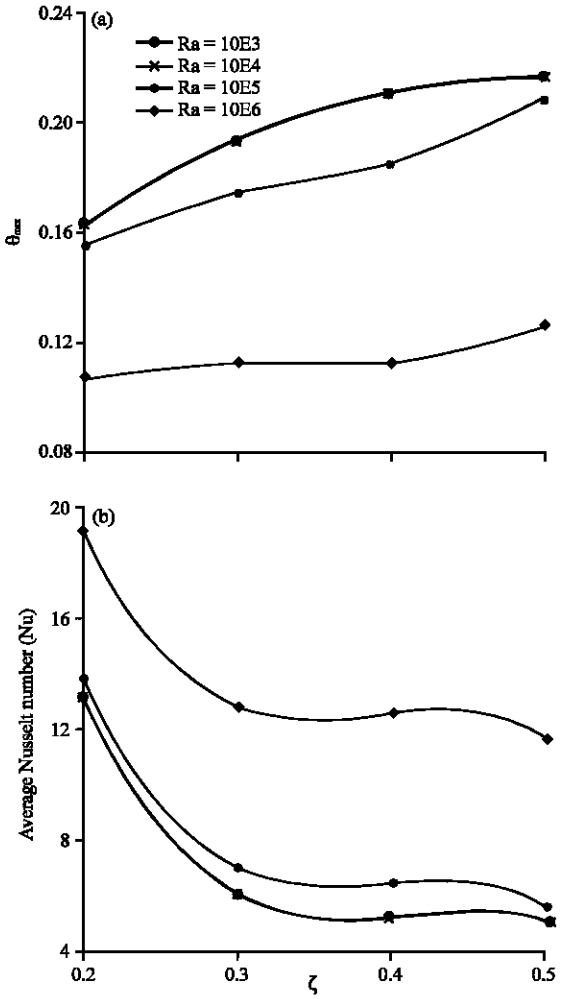

Fig. 15: Combine effects of Rayleigh number and position of heating element on: a) Maximum temperature and b) Average Nusselt number under at $\varepsilon = 0.4$ and $\varphi = 0.1$

also from ($\Pi_{max} = 0.04436$) to ($\Pi_{max} = 0.20356$) for nanofluid. In other words, moving the heating element from left sidewall to the middle of the lower wall causes an increase in the heat transfer in the enclosure. Consequently, the direction of the heat transfer path represented by heatlines changes from the hot lower wall (heating element) towards the cold vertical walls.

Maximum temperature and average Nusselt number: Figure 15 points out the maximum temperature and average Nusselt number with respect to effect of position of heat element (ζ) and Rayleigh number at $\varepsilon = 0.4$ and $\varphi = 0.1$. As shown in Fig. 15a, the maximum temperature is a function of heat element position (ζ) for different Rayleigh numbers. When the isoflux heating

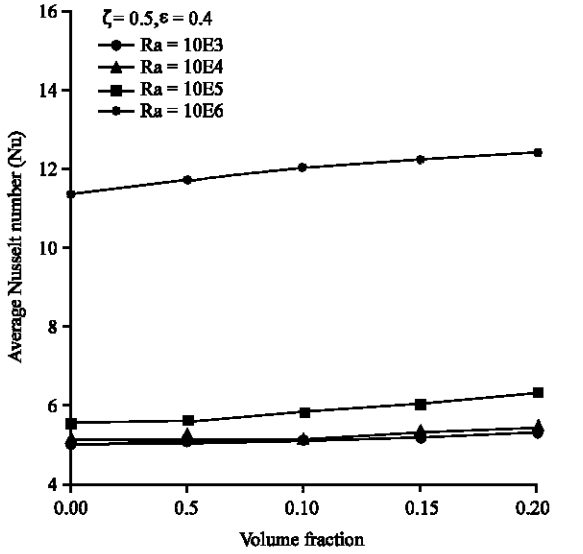

Fig. 16: Average Nusselt number at different values of nanofluid volume fraction for different Rayleigh number

element moves to the mid-section of the lower wall, the max. temperature increases for fixed Ra number and it decreases with increasing values of Rayleigh number. Figure 15b reveals the average Nusselt number versus heating element position (ζ) for different Ra numbers at $\varepsilon = 0.4$ and $\varphi = 0.1$. In general case, the average Nu increases with increasing of Ra due to enhanced convection, especially, for higher values of Ra (10^5-10^6), while for lower values of Ra (10^3-10^4), the average Nu is nearly invariant due to the diffusion dominated heat transfer. Furthermore, the values of average Nusselt number decrease as heat element positions increase from $\zeta = 0.2L$ to $\zeta = 0.5L$ for whole cases. When Ra equals to 10^5, the values of $\overline{Nu}$ number are higher than previous cases (10^3 and 10^4) due to an augmentation in effective fluid motion. Conversely, the average Nusselt numbers reduce as ζ rises from 0.2-0.5L but with a smaller slope than that of lower Rayleigh numbers. The values of the number are obviously shown for high Ra number (10^6). Significantly, minimum values of Nu are observed at $\zeta = 0.5L$ at every Rayleigh numbers.

Figure 16 shows the relationship between $\overline{Nu}$ number and nanopartice volume fraction for different Ra numbers at $\varepsilon = 0.4$, $\zeta = 0.5L$. At lower values of Ra number (10^3 and 10^4), the values of the $\overline{Nu}$ number increase for whole values of nanoparticle volume fraction. As value of Ra increases to10^5, higher values of the $\overline{Nu}$ number are observed with high slope than that for lower Ra (10^3 and 10^4). At higher value of Ra number (10^6), the slope of $\overline{Nu}$ number line is observed nearly zero.

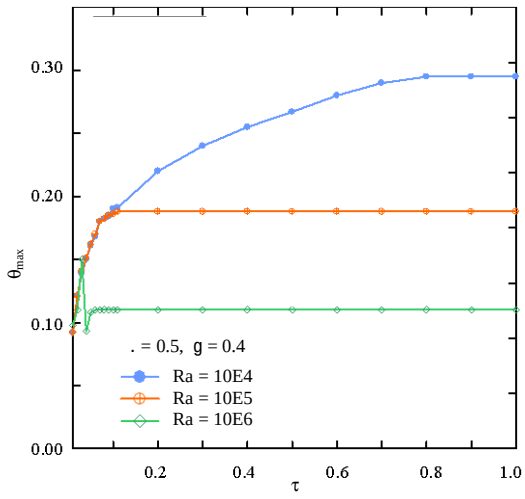

Fig. 17: Time histories of θ maximum heat source temperature (ε = 0.4, ζ = 0.5L and φ = 0.1) for different Rayleigh number

Figure 17 displays the impermanent variations of maximum temperature of the isoflux heating element. The flow development is classified into three periods which are an initial period, a transitional period and a steady period. In the initial period, a sudden isoflux heating element leads to growth of a thermal layer at the neighboring source. Figure 17 also depicted that the dimensionless maximum temperature starts to be steady at time histories equal to 0.1 for Rayleigh numbers ranging from 10^5-10^6 while maximum temperature reaches to steady for Rayleigh number 10^4 when time histories increase to 0.8.

CONCLUSION

This research visualizes the heat flow for unsteady natural convection inside a square enclosure filled with pure water and Cu-water nanofluid using heatline approach. Also, study aims to investigate the effects of Rayleigh numbers and the solid volume fraction of nanoparticles as well as effects of position of isoflux heating element and length ratio of heating element (ε) on the thermal and flow fields. The right and left vertical walls of the enclosure are subjected to cooled temperature and the bottom wall is subjected to constant flux heating element while the upper wall and circular cylinder are insulated. The implicit finite element technique is used to solve this problem. From the obtained results, we concluded the following important points:

The flow strength reduces when the solid volume fraction rises for all values of Ra number. When the dimensionless time increases, temperature gradient also increases. Maximum temperature reduces with raising both Ra number and solid volume fraction. An increase of the solid volume fractions from 0-0.2 results increasing in the average Nu for all values of Ra number. The values of the heat function increase for both pure water and nanofluid for enclosure when the heating element position moves from the left sidewall to the mid-section of bottom wall. The average Nu decreases with increasing heat element positions (ζ) but maximum temperature (θ_{max}) increases with increasing positions of heat element. The time needed to reach the steady state is longer for lower Ra numbers and shorter for higher Ra numbers.

REFERENCES

Abu-Nada, E., Z. Masoud, H.F. Oztop and A. Campo, 2010. Effect of nanofluid variable properties on natural convection in enclosures. Intl. J. Therm. Sci., 49: 479-491.

Alsabery, A.I., A.J. Chamkha, H. Saleh and I. Hashim, 2017. Transient natural convective heat transfer in a trapezoidal cavity filled with non-Newtonian nanofluid with sinusoidal boundary conditions on both sidewalls. Powder Technol., 308: 214-234.

Aminossadati, S.M. and B. Ghasemi, 2009. Natural convection cooling of a localised heat source at the bottom of a nanofluid-filled enclosure. Eur. J. Mech. B Fluids, 28: 630-640.

Basak, T., G. Aravind, S. Roy and A.R. Balakrishnan, 2010a. Heatline analysis of heat recovery and thermal transport in materials confined within triangular cavities. Intl. J. Heat Mass Transfer, 53: 3615-3628.

Basak, T., S. Roy, A. Matta and I. Pop, 2010b. Analysis of heatlines for natural convection within porous trapezoidal enclosures: Effect of uniform and non-uniform heating of bottom wall. Intl. J. Heat Mass Transfer, 53: 5947-5961.

Brinkman, H.C., 1952. The viscosity of concentrated suspensions and solutions. J. Chem. Phys., 20: 571-581.

Choi, S.U.S. and J.A. Eastman, 1995. Enhancing thermal conductivity of fluids with nanoparticles. Proceedings of the International Mechanical Engineering Congress and Exposition, November 12-17, 1995, San Francisco, CA., USA., pp: 99-105.

Costa, V.A.F. and A.M. Raimundo, 2010. Steady mixed convection in a differentially heated square enclosure with an active rotating circular cylinder. Intl. J. Heat Mass Transfer, 53: 1208-1219.

Ghahremani, E., 2018. Transient natural convection in an enclosure with variable thermal expansion coefficient and nanofluid properties. J. Appl. Comput. Mech., 4: 133-139.

Ghasemi, B. and S.M. Aminossadati, 2010b. Brownian motion of nanoparticles in a triangular enclosure with natural convection. Int. J. Thermal Sci., 49: 931-940.

Ghasemi, B. and S.M. Aminossadati, 2010a. Periodic natural convection in a nanofluid-filled enclosure with oscillating heat flux. Intl. J. Therm. Sci., 49: 1-9.

Hussein, A.K. and S.H. Hussain, 2016. Heatline visualization of natural convection heat transfer in an inclined wavy cavities filled with nanofluids and subjected to a discrete isoflux heating from its left sidewall. Alexandria Eng. J., 55: 169-186.

Jmai, R., B. Ben-Beya and T. Lili, 2013. Heat transfer and fluid flow of nanofluid-filled enclosure with two partially heated side walls and different nanoparticles. Superlattices Microstruct., 53: 130-154.

Khodadadi, J.M. and S.F. Hosseinizadeh, 2007. Nanoparticle-Enhanced Phase Change Materials (NEPCM) with great potential for improved thermal energy storage. Intl. Commun. Heat Mass Transfer, 34: 534-543.

Mahmoodi, M. and S.M. Sebdani, 2012. Natural convection in a square cavity containing a nanofluid and an adiabatic square block at the center. Superlattices Microstruct., 52: 261-275.

Maxwell, J., 1904. A Treatise on Electricity and Magnetism. 2nd Edn., Oxford University Press, Cambridge, UK.,.

Mohebbi, R., M. Izadi and A.J. Chamkha, 2017. Heat source location and natural convection in a C-shaped enclosure saturated by a nanofluid. Phys. Fluids, 29: 1-13.

Nguyen, M.T., A.M. Aly and S.W. Lee, 2016. Unsteady natural convection heat transfer in a nanofluid-filled square cavity with various heat source conditions. Adv. Mech. Eng., 8: 1-18.

Oztop, H.F. and E. Abu-Nada, 2008. Numerical study of natural convection in partially heated rectangular enclosures filled with nanofluids. Int. J. Heat Fluid Flow, 29: 1326-1336.

Oztop, H.F., M.M. Rahman, A. Ahsan, M. Hasanuzzaman, R. Saidur, K. Al-Salem and N.A. Rahim, 2012. MHD natural convection in an enclosure from two semi-circular heaters on the bottom wall. Int. J. Heat Mass Transfer, 55: 1844-1854.

Oztop, H.F., P. Estelle, W.M. Yan, K. Al-Salem and J. Orfi *et al.*, 2015. A brief review of natural convection in enclosures under localized heating with and without nanofluids. Intl. Commun. Heat Mass Transfer, 60: 37-44.

Putra, N., W. Roetzel and S.K. Das, 2003. Natural convection of nano-fluids. Heat Mass Transfer, 39: 775-784.

Rahman, M.M., H.F. Oztop, A.H. Joarder, R. Saidur, N. Hamzah, K. Al-Salem and T.A. Ibrahim, 2016. Unsteady Analysis of Natural Convection in a Carbon nanotube-water Filled Cavity with Inclined Heater. Numer. Heat Transfer Part, 69: 794-809.

Rahman, M.M., H.F. Oztop, S. Mekhilef, R. Saidur and K. Al-Salem, 2014. Unsteady natural convection in Al_2O_3-water nanoliquid filled in isosceles triangular enclosure with sinusoidal thermal boundary condition on bottom wall. Superlattices Microstruct., 67: 181-196.

Roslan, R., H. Saleh and I. Hashim, 2014. Natural convection in a differentially heated square enclosure with a solid polygon. Sci. World J., 2014: 1-11.

Saeid, N.H., 2018. Natural convection in a square cavity with discrete heating at the bottom with different fin shapes. Heat Transfer Eng., 39: 154-161.

Sivasankaran, S. and K.L. Pan, 2014. Natural convection of nanofluids in a cavity with nonuniform temperature distributions on side walls. Numer. Heat Transfer Part A. Appl., 65: 247-268.

Xie, H., J. Wang, T. Xi, Y. Liu and F. Ai, 2002. Dependence of the thermal conductivity on nanoparticle fluid mixture on the base fluid. J. Mater. Sci. Lett., 21: 1469-1471.

Xuan, Y. and Q. Li, 2000. Heat transfer enhancement of nanofluids. Int. J. Heat Fluid Flow, 21: 58-64.

Yoo, J.S., 1998. Mixed convection of air between two horizontal concentric cylinders with a cooled rotating outer cylinder. Intl. J. Heat Mass Transfer, 41: 293-302.

Zhao, F.Y., D. Liu and G.F. Tang, 2007. Conjugate heat transfer in square enclosures. Heat Mass Transfer, 43: 907-922.